

AMINPENTACIANOFERRATO COMO INDICADOR DE MONÓXIDO DE CARBONO

AMINPENTACYANOFERRATE AS A CARBON MONOXIDE INDICATOR

Camilla Ferradoza Batalioto¹

Caroline Pauletti²

Dheniffer Sandra de Oliveira Buffon³

Douglas Cardoso Dragunski⁴

Cleber Antonio Lindino⁵

Resumo: O monóxido de carbono (CO) é uma substância que pode causar asfixia e morte e uma de suas principais fontes é a emissão de gases no escapamento de veículos automotores, devido à combustão incompleta. Por isso, vários países têm importante legislação sobre poluição veicular. Diversas técnicas analíticas para determinação do CO são utilizadas, porém, em sua maioria, são dispendiosas ou necessitam de profissionais qualificados. A proposta deste trabalho foi utilizar o complexo aminpentacianoferrato no desenvolvimento de metodologia espectrofotométrica a partir da troca de ligante amônia (NH₃) pela carbonila (CO), com aplicabilidade na determinação rápida de monóxido de carbono em emissões veiculares. O complexo sintetizado foi caracterizado quanto à sua estrutura e os parâmetros analíticos foram validados. A curva analítica situou-se entre 135 mg L⁻¹ e 812 mg L⁻¹, com R² = 0,9965, com repetitividade de 4,6% e estabilidade do complexo carbonilado de ±1,0% em 15 minutos. Este método foi aplicado em amostras de gás de emissão veicular possuindo baixo custo, podendo-se utilizar espectrofotômetros portáteis de fácil manipulação e de acesso, para medidas rápidas.

Palavras-chaves: Poluente. Saúde pública. Nitroprussiato. Veículo.

Abstract: Carbon monoxide (CO) is a substance that can cause suffocation and death and one of its main sources is the emission of gases in the exhaustion of motor vehicles, due to incomplete combustion. For this reason, several countries have passed important legislation on vehicular pollution. Several analytical techniques for determining CO are used; however, most of them are expensive or require qualified professionals. The purpose of this work was to use the aminpentacyanoferrate complex in the development of a spectrophotometric methodology based on the exchange of ammonia ligand (NH₃) by carbonyl (CO), with applicability in the rapid determination of carbon monoxide in vehicle emissions. The synthesized complex was characterized in terms of its structure and the analytical parameters were validated. The analytical curve was between 135 mg L⁻¹ and 812 mg L⁻¹, with R² = 0.9965, with a repeatability of 4.6% and stability of the carbonylated complex of ± 1.0% in 15 minutes. This method was applied to samples of vehicle emission gas, performing at low cost and being possible to use portable spectrophotometers of easy manipulation and access, for fast measurements.

Keywords: Pollutant. Public health. Nitroprusside. Vehicle.

¹ Universidade Estadual do Oeste do Paraná, Campus Toledo – Brasil. In memorian

² Universidade Estadual do Oeste do Paraná, Campus Toledo – Brasil. carol_pauletti@hotmail.com

³ Universidade Estadual do Oeste do Paraná, Campus Toledo – Brasil. dhenifferbuffon1@gmail.com

⁴ Universidade Estadual do Oeste do Paraná, Campus Toledo – Brasil. dcdragunski@gmail.com

⁵ Universidade Estadual do Oeste do Paraná, Campus Toledo – Brasil. lindino99@gmail.com

1 Introduction

Carbon monoxide (CO) is a colorless and odorless gas, highly toxic, emitted mainly by the combustion of fuels and other organic materials in environments with a limited amount of oxygen. In living organisms exposed to carbon monoxide, oxygen transport to cells is limited and dizziness, headaches, nausea, unconsciousness, and death are observed at high levels (DOWNS, 2016; TÉLLEZ; RODRÍGUEZ; FAJARDO, 2016). Daily exposure to CO from the environment has been associated with an increase in hospital admissions, particularly for individuals with cardiovascular diseases, which can lead to premature death (REBOUL et al., 2017). The World Health Organization (WHO) estimates that air pollution was responsible for 4.2 million deaths in 2016 (WHO, 2016).

Assessing the concentration of air pollutants, especially carbon monoxide (CO), is important to predict the impact on human health and the environment. To allow the management and control of pollutants, seasonal variations of meteorological parameters and the factors that influence these changes must be identified, such as topographic structure and urban heat islands as well as temperature inversion and changes in solar radiation and air pollutants sources (SAFARIANZENGIR et al., 2020). For the control of CO pollution, the EU guidelines established the maximum CO limit of 10 mg m^{-3} (EC, 2008). In Brazil, the limit established is 10.31 mg m^{-3} (9 ppm) (BRAZIL, 2018).

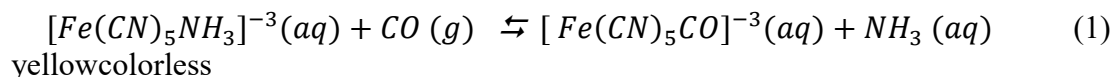
Motor vehicles are largely responsible for CO (YANG; SHEN; LIANG, 2020; ZDZISŁAW et al., 2020) and the low quality and insufficient quantity of public transport are the main reasons for the growth of the fleet of private vehicles in the metropolitan regions (GARCIA et al., 2013). It is estimated that the best-selling vehicles in Brazil generate between 0.403 to 0.960 g km^{-1} of CO, while motorcycles produce between 0.680 to 0.723 g km^{-1} (GARCIA et al., 2013). Specifically, in the State of São Paulo, which has the largest fleet of vehicles and has intense industrialization, CO levels in the atmosphere reached 315×10^3 tons in 2018, with vehicles accounting for 96.5% of CO (GUARDANI; MURAMOTO, 2019).

The Brazilian Motor Vehicle Air Pollution Control Program (PROCONVE) establishes that the maximum limit of carbon monoxide emission from the exhaust of light passenger vehicles, for road use, is 1.30 g km^{-1} , being idling for an Otto cycle engine is 0.3% by volume (BRAZIL, 2009). The measurement of the emission of pollutants from the exhaust of light passenger vehicles and light commercial vehicles follows Brazilian Regulation, NBR 6601/2012, and the criteria established in Resolution No. 18/1986, of the National Environment Council (CONAMA) (BRAZIL, 1986; BRAZIL, 2012).

In the literature, the determination of carbon monoxide from automotive vehicle emissions involves the use of portable gas sensors (ABI-ESBER; EL-FADEL; SHIHADDEH, 2007; KACEMA et al. 2018); gas chromatography with thermal conductivity detector (ZUAS; BUDIMAN, 2015); semiconductor sensors (POCHWAŁA et al., 2020); infrared spectrophotometry (BRAZIL, 1995) and automatic multi-analyzers (PAPADOPOULOS, 2020; SEVINC; HAZA, 2020; ZHUA et al., 2020), many of which are difficult to use for *in situ* measures, with the high cost and, therefore, difficult to be widely disseminated.

Spectrophotometric measurements in the visible region can be attractive due to their ease of use, lower cost, and the control of selective reactions to the desired analyte. The absorption of carbon monoxide in solution containing the yellow aminopentacyanoferrate complex $[\text{Fe}(\text{CN})_5\text{NH}_3]^{-3}$ is accompanied by the discoloration of the solution (Equation 1), making it possible to monitor it by visible spectrophotometry (KENNEY; FLYNN; GALLINI, 1961). The carbonylated complex does not absorb in the visible region and the decrease in the absorbance of the aminopentacyanoferrate complex can be correlated to the

concentration of carbon monoxide that reacts with it. The reaction is made possible by the fact that CO is a strong field ligand of the spectrochemical series, which easily replaces the NH₃ ligand in the complex structure.



The interaction of the potassium aminpentacyanoferrate complex with carbon monoxide and its application as an analytical tool has not been explored and, therefore, this work had the objective of evaluating this complex in the determination of CO gas in vehicular emission, for quick, easy measurements, perform and low cost.

2 Materials and methods

All chemical reagents used were of purity grade for analysis. The water used to prepare standard solutions or sample dilutions was purified by ion exchange (Lucaderma, Brazil) and Simplicity Milli-Q system (Millipore, USA). The gases Argon (White Martins, Brazil - 99.999%), Hydrogen (White Martins, Brazil - 99.999%), Nitrogen (Linde, Brazil - 99.999%), Methane (AGA, Brazil - 99.995%), Carbon Monoxide (White Martins, Brazil - 99.5%) and carbon dioxide (Linde, Brazil - 99.9%) were used in the interaction tests with the complex. The ammonia gas was generated from a 30% v/v reagent solution (Carlo Erba) using soft heating at 40 °C.

The K₃[Fe(CN)₅(NH₃)]·3H₂O was synthesized according to the procedure described in the literature, with adaptations (KENNEY; FLYNN; GALLINI, 1961). In a closed borosilicate glass flask, 3 g of potassium nitroprusside (K₂[Fe(CN)₅NO]·2H₂O), pulverized in a mortar, were dissolved in 12 mL of 30% v/v ammonium hydroxide (Carlo Erba). Then, 1g of anhydrous potassiumacetate was added to the flask and the solution was kept in a thermostatic bath at 10 ± 1 °C for 10 hours. The yellow solid formed was separated by vacuum filtration and then redissolved in a minimum amount of water at 5.0 °C and re-precipitated with 95% v/v ethanol (Vetec) at 5.0 °C. The mixture was again filtered in vacuum and the resulting solution remained refrigerated at 10 ± 1 °C, adding 95% v/v cold ethanol to precipitate the rest of the complex. The solid formed was collected by filtration, washed with cold ethanol, and kept under vacuum in a desiccator with silica gel for seven days. The synthesis yield was 60%.

The complex obtained was characterized in an aqueous solution in the UV-visible region in a Shimadzu® UV1800-PC spectrophotometer double beam, with scanning between 200 and 1100 nm with resolution ± 1 nm in a 10 mm optical path quartz cuvette.

Spectroscopy analysis in the Infrared region was performed on an FTIR PerkinElmer® Frontier. The sample was prepared using KBr tablets dried at 105 °C for one hour, with 2% w/w of the sample of the complex and analyzed between 4000 and 500 cm⁻¹, with a resolution of 2.0 cm⁻¹ and 10 successive scans in each measurement.

The Thermogravimetric Analysis (TGA) was performed in PerkinElmer® STA 6000 between temperatures of 30 °C to 900 °C with a heating gradient of 10 °C min⁻¹ and nitrogen flow of 50 mL min⁻¹ obtaining also the derivative TGA (DTGA). Differential Scanning Calorimetry (DSC) was performed on Shimadzu® DSC-60 equipment with scanning at temperatures between 30 °C and 500 °C with a heating gradient of 10 °C min⁻¹ and nitrogen flow of 50 mL min⁻¹.

The electrochemical characterization was performed by cyclic voltammetry of the aminpentacyanoferrate complex at a concentration of 2.6 x 10⁻³ mol L⁻¹ in KNO₃ 0.2 mol L⁻¹

medium as support electrolyte, at a temperature of 25 °C, with scanning of 50 mV s⁻¹ in EG&G PAR[®] 273A potentiostat with a platinum working electrode, saturated Ag/AgCl/KCl electrode and platinum auxiliary electrode, between potentials from -0.2 to +0.7 V. The carbonylated complex was obtained by bubbling CO (White Martins, 99.5%) in the supporting electrolyte for 20 minutes and performing cyclic voltammetry with the same parameters.

To evaluate the effect of the electrolyte on the absorbance response, the absorption spectra of the complex in the visible region at different concentrations were obtained in aqueous solution, in a 0.1 mol L⁻¹ NaOH solution, in a TRIS-HCl 0.1 mol L⁻¹ buffer solution pH 7.0 and phosphate buffer 0.1 mol L⁻¹ pH 7.0.

The interaction of the complex with different gases (CH₄, CO₂, CO, NH₃) was evaluated by spectrophotometry in the UV-visible region, under the same conditions as the characterization, after bubbling the gases for 20 minutes in the aqueous solution of the complex in the concentration of 2.6 x 10⁻³ mol L⁻¹. Synthetic air and N₂ were used as a comparison.

For the analytical tests to determine CO gas, hypodermic syringes containing 3 mL of the complex solution (2.6 x 10⁻³ mol L⁻¹) were used, adding 1.5 mL of the gas to be studied (except for the study of the effect of concentration), and each syringe was shaken for two minutes and the absorbance was read on the Shimadzu UV-visible Spectrophotometer. In all measurements, the air temperature was measured with an Incoterm digital thermometer (± 0.5 °C) and the local atmospheric pressure was recorded using Simepar¹ data for calculating the quantity of substance (mol) and gas concentration. The measurements were made in duplicate.

To evaluate the influence of the factors of the concentration of the complex, temperature, and agitation time in the reaction between the complex and CO, the factorial design 2³ (duplicate) was used. The test parameters are described in Table 1.

Table 1 - Factorial design. C = concentration of the complex; T = temperature; t = stirring time.

Fa ctors		
C (mol L ⁻¹)	.0013	.0052
T (°C)	5.0	5.0
t (s)	0	20

The analytical curve was obtained using hypodermic syringes containing 3 mL of the aqueous solution of the complex (2.6 x 10⁻³ mol L⁻¹) with the addition of 0 mL; 0.5 mL; 1.0 mL; 1.5 mL and 2 mL of standard CO (White Martins, 99.5%), shaking each syringe for two minutes and reading the absorbance on the Shimadzu UV-visible Spectrophotometer. All points were made in duplicate.

The repeatability test was carried out using three levels of monoxide concentration (135; 400 and 680 mg L⁻¹ of CO) in aminopentacyanoferrate 2.6 x 10⁻³ mol L⁻¹ solution, shaking the collection for two minutes after injection, totaling nine experiments (three for each concentration of CO).

In all experiments, the gases were collected directly from the cylinder using a Tedlar[®]

¹Parana Technology and Environmental Monitoring System. Available at <http://www.simepar.br/>.

bag (polyvinyl fluoride), which was used to collect the syringes. All tests were performed in duplicate.

The proposed methodology was applied in the determination of CO in vehicle emission gases, according to the Brazilian environmental standard (BRAZIL, 2012). The collection equipment used in the tests was developed in the laboratory and consists of an oil suction pump (12 V) adapted to suck in the vehicle emission gas, with a heat resistant pipe of 2 meters in length and wiring with plugs for connection in the car battery, eliminating the need for a power source external to the vehicle. The gas pump flow was set at $3.34 \pm 0.03 \text{ L min}^{-1}$ (RSD = 0.90%, n = 5).

The sampling procedure consisted of inserting 30 cm of the pipe into the vehicle's exhaust and starting the vehicle, manufactured in 2012, gasoline, keeping the rotation in idle for one minute, and collection in Tedlar[®] bag, previously cleaned with N₂ inert gas (White Martins, 99.999%), was carried out at 2,500 rpm after stabilization for one minute.

1.5 mL of the vehicle emission gas sample was collected from the gas in the bag, in duplicate, in hypodermic syringes using 3 mL of the aqueous solution or 0.1 mol L⁻¹ NaOH solution of the complex in a concentration of $2.6 \times 10^{-3} \text{ mol L}^{-1}$; with the addition of 1.5 mL of standard carbon monoxide gas with stirring for two minutes and the absorbance was measured at $\lambda=400 \text{ nm}$ in a UV-visible spectrophotometer. In all measurements, the air temperature was measured with an Incoterm digital thermometer ($\pm 0.5 \text{ }^{\circ}\text{C}$), and the local atmospheric pressure was recorded and the CO concentration in mg L⁻¹, ppm, and % was calculated through Equation 2.

$$C_x = \frac{A_1 \cdot C_p \cdot V_p}{A_2 \cdot V_t - A_1 \cdot V_1} \quad (2)$$

where A_1 corresponds to the absorbance of the sample (without the addition of a standard), C_p is the concentration of the standard, V_p represents the volume of standard added to the second point, A_2 is the absorbance of the sample with the addition of standard, V_t is the total volume of the solution, V_1 the volume of sample added.

The vehicle emission gas was characterized in the infrared region in an FTIR PerkinElmer[®] Frontier Spectrometer, between 4000 and 500 cm⁻¹, with a resolution of 2 cm⁻¹ and 10 successive scans in a gas cell with zinc selenide windows. Before and between measurements, the gas cell was purged with N₂ (White Martins, 99.999%) for cleaning.

After saturation with the gases, the pH of the solutions was determined using BEL pH meter (model PHS3BW), calibrated with buffer solution pH 4.00 ± 0.02 and pH 7.00 ± 0.02 .

3 Results and discussion

Figure 1 shows the absorption spectra of the complex in aqueous medium.

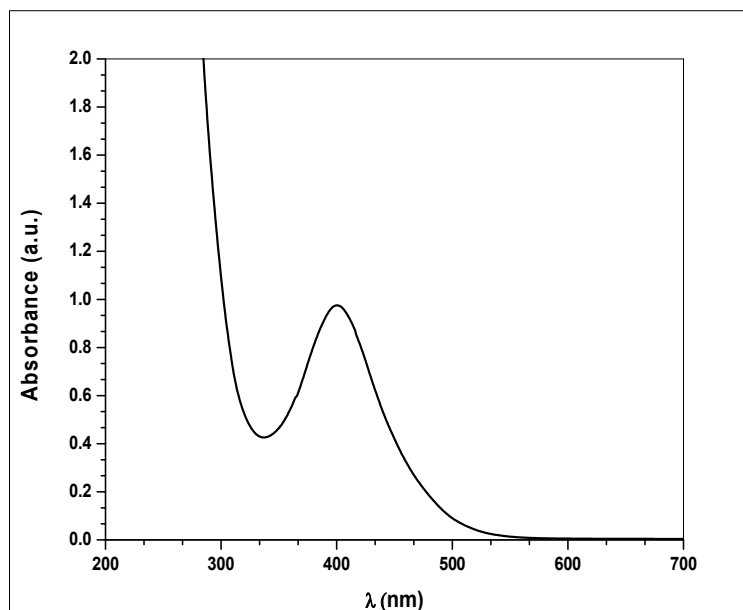


Figure 1. Molecular absorption spectrum in the ultraviolet-visible region of $K_3[Fe(CN)_5(NH_3)].3H_2O$ in aqueous solution, at a concentration of $2.6 \times 10^{-3} \text{ mol L}^{-1}$. Temperature of 25.0°C .

The maximum absorption of the complex in the visible region occurs at 400 nm, also presenting strong absorption in the ultraviolet region. The 400 nm band is attributed to the d-d transitions in the metal ion (BARAN; MULLER, 1969). The band that occurs at 220 nm (not shown) has a high intensity and has been attributed to charge transfer transitions involving the central ion and the cyanide ligands (PAVIA et al., 2010). The spectrum for potassium nitroprusside shows an absorption shoulder at 271 nm for the nitro group and 222 nm attributed to the strong absorption of cyan groups (PAVIA et al., 2010).

The vibrational spectrum in the mid-infrared region of the complex is shown in Figure 2.

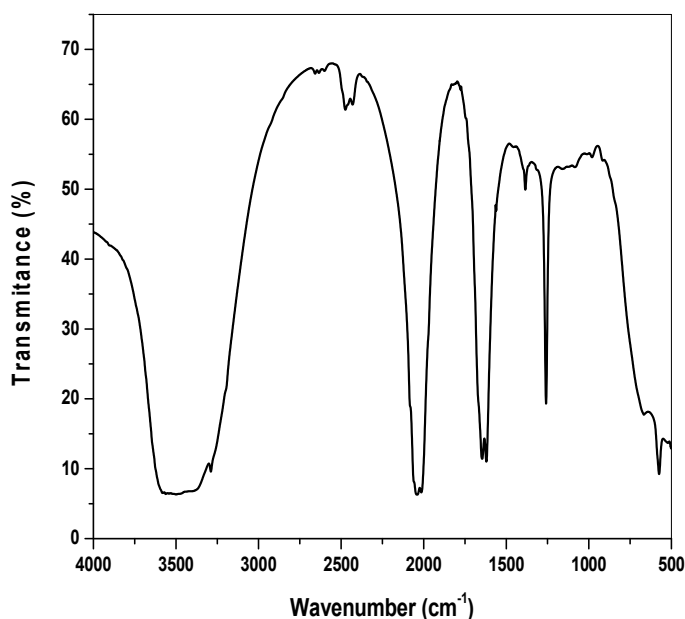


Figure 2. Vibrational spectrum of the complex $K_3[Fe(CN)_5NH_3] \cdot 3H_2O$ in the mid-infrared.

The assignments to the vibrational spectrum in the infrared region have mainly referred to C–N stretches and Fe–C–N deformations. The Fe–L, and Fe–C stretch bands are generally of low intensity and often covered by more intense bands. Table 2 presents the frequency values for the studied complex and the values found in the literature that corroborate the results.

Table 2 - Absorption data for the complex potassium aminopentacyanoferrate in the mid-infrared.

Wavenumber (cm ⁻¹)	Assignment	References ^a
3578-3368	OH	35
		50-3200
3290	NH	32
	3	88
2030	C≡N	20
	N	42
1645	NH	16
	3	49
1260	NH	12
	3	58
577	Fe-CN	57
		4

^aReferences: (SILVERSTEIN; WEBSTER; LIEMLE, 2006; PAVIA et al., 2010)

Figure 3 shows the thermogravimetric curves and their derivatives for the complex and the starting reagent, nitroprusside.

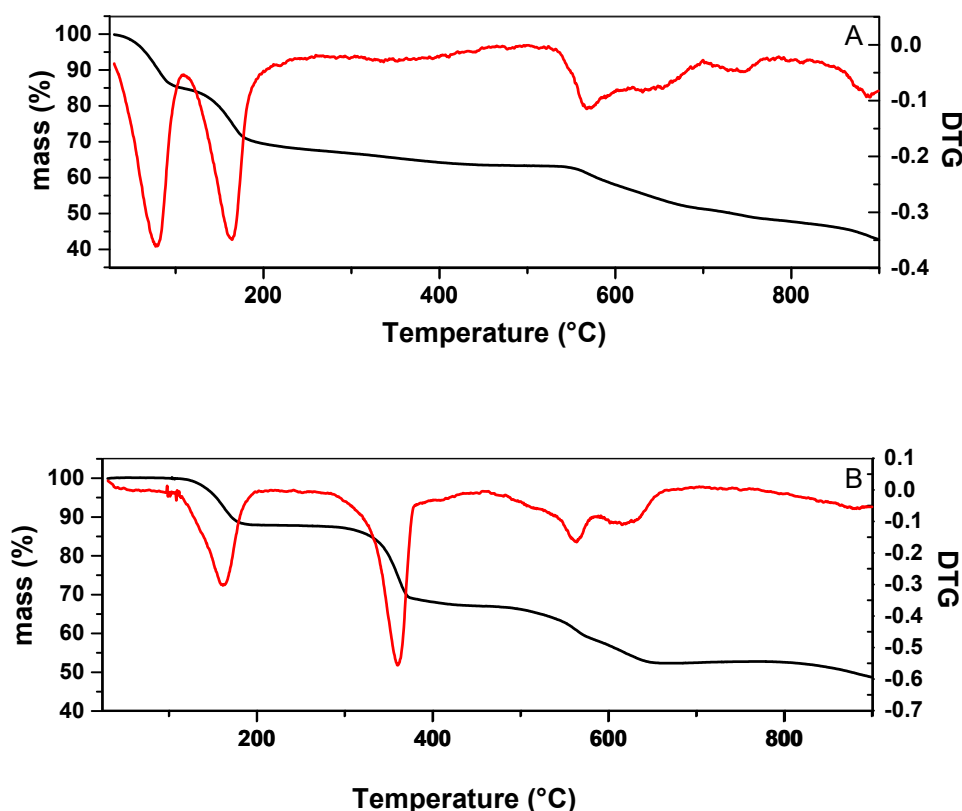
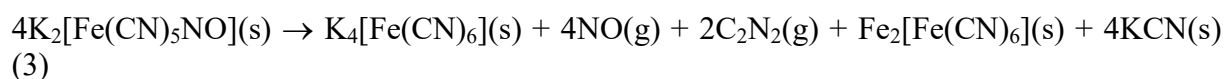


Figure 3. Thermogravimetric curves (—) and derived from the degradation curves (—). A) aminopentacyanoferrate; B) potassium nitroprusside. The heating gradient of 10 °C min⁻¹ and nitrogen flow of 50 mL min⁻¹.

In the thermogravimetric curve of the complex (Figure 3A), three main thermal events are observed. The first two at 90 °C and 180 °C refer to the loss of hydration water molecules, which corresponds to 14.2% of the mass. The third event occurs from 180 °C and occurs in two stages, with a loss of mass of 15% attributed to aminoacetonitrile (HN=CHCN) and loss of mass of 7.8%, attributed to the formation of N₂. The final mass was 42.5% of the initial mass, represented by residues of potassium cyanides, iron carbide, and graphite (AMAULY; VARETTI; AYMUNINO, 1985; AMAULY; VARETTI; AYMUNINO, 1986).

The nitroprusside thermogravimetric curve (Figure 3B) shows thermal events between 110 and 179 °C and refers to the loss of two hydration water molecules, which corresponds to 12.1% of the mass. The second event between 180 to 376 °C refers to losses of cyanogen (C₂N₂) and NO with a loss of mass of 33% and the event between 376 and 650 °C, also refers to the formation of cyanogens. The mass of the residue corresponds to 48.7% of the initial mass, represented by residues of potassium cyanides and hexacyanoferrates. Equation 3 shows the proposed decomposition reaction (BALA; DASU; MIHAILCIUC, 2013).



The DSC results for the complex and nitroprusside are shown in Figure 4.

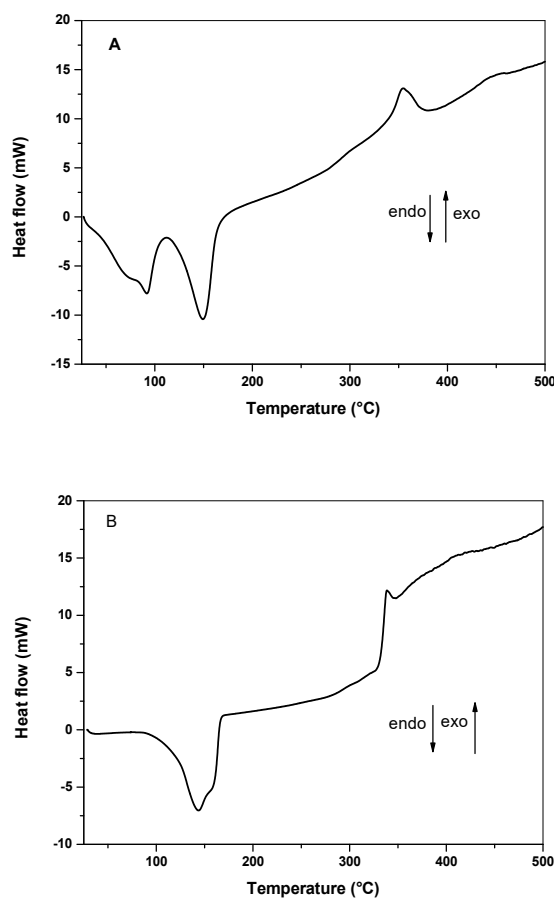
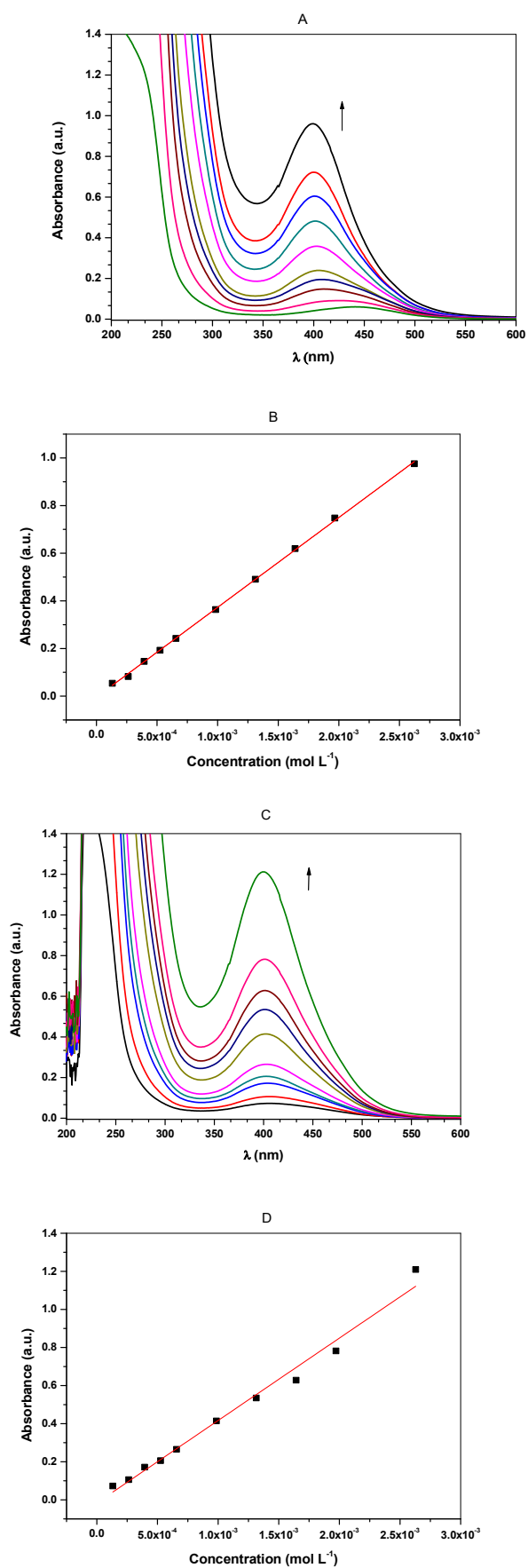


Figure 4. Differential scanning calorimetry curve for A) aminopentacyanoferrate; B) potassium nitroprusside. Heating gradient of $10\text{ }^{\circ}\text{C min}^{-1}$ and nitrogen flow 50 mL min^{-1} .

For the complex (Figure 4A), the first endothermic peak at $92\text{ }^{\circ}\text{C}$ and the second endothermic peak at $149\text{ }^{\circ}\text{C}$ refer to the loss of hydration water molecules. The exothermic peak refers to the crystallization of the complex that takes place at approximately $353\text{ }^{\circ}\text{C}$. For nitroprusside (Figure 4B), there is only one endothermic peak at $143\text{ }^{\circ}\text{C}$ for water losses and an exothermic peak at $339\text{ }^{\circ}\text{C}$ for nitroprusside crystallization.

Figure 5 shows the spectra of the complex in different electrolytes to evaluate the spectrophotometric response under different conditions. Table 3 presents the equations of the curves obtained and the coefficient of determination in the absorbance response with the concentrations in each electrolyte studied.



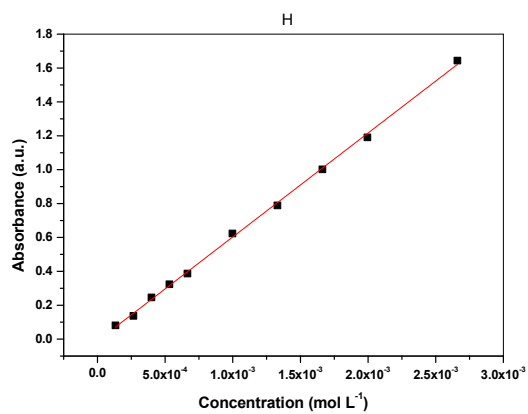
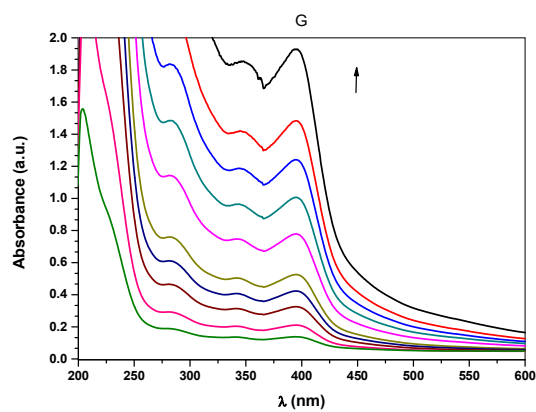
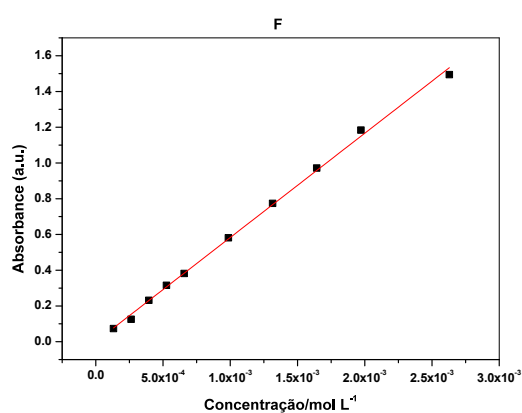
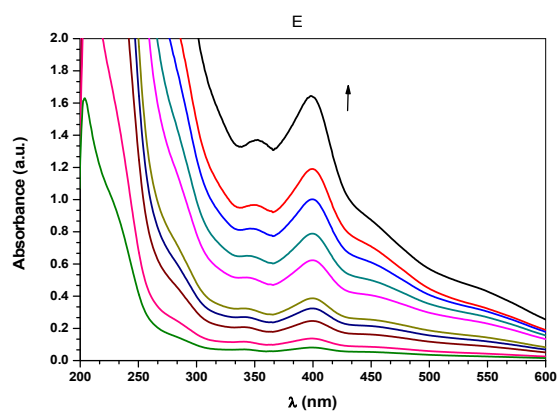
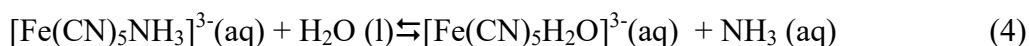


Figure 5. Molecular absorption spectra of the aminopentacyanoferrate at different concentrations (the arrow indicates the increase in concentration) and the respective absorbance response curves at $\lambda = 400$ nm. A-B: purified water; C-D: 0.1 mol L⁻¹ NaOH solution; E-F: buffer solution Tris-HCl 0.1 mol L⁻¹ pH 7.0; G-H: 0.1 mol L⁻¹ pH 7.0 phosphate buffer solution. Temperature of 25.0 °C.

Table 3 - Equations of the curves for variation of the concentration of the aminopentacyanoferrate in different electrolytes and respective coefficients of determination (R^2).

Electrolyte	Equation	R^2
Purified water	$y = -0,00415 + 377.022x$.999
NaOH 0.1 mol L ⁻¹	$y = -0.01597 + 432.679x$.988
Tris-HCl 0.1 mol L ⁻¹ pH 7.0	$Y = 0.000151 + 613.352x$.998
Phosphate 0.1 mol L ⁻¹ pH 7.0	$y = -0.01039 + 613.352x$.999

In aqueous solution (Figure 5A) the displacement of the wavelength from a maximum of 440 to 400 nm occurs with an increase in the concentration of the aminopentacyanoferrate complex, which may be associated with the balance of Equation 4 with the exchange of H₂O and NH₃ ligands; in low concentrations of the complex, the species $[\text{Fe}(\text{CN})_5\text{H}_2\text{O}]^{3-}$ is favored.



In Tris-HCl and phosphate buffer solutions, peaks appear at 352 and 203 nm and 348, 283, and 203 nm, respectively, which distort the maximum absorption curve and may compromise the accuracy of the method. Besides, there is the displacement of the baseline by scattering of light, due to the appearance of turbidity in the solution, indicating the partial decomposition of the complex, catalyzed by the presence of dissolved oxygen, pH, and light, which can generate Prussian Blue (KENNEY; FLYNN; GALLINI, 1961). In NaOH solution, there is no displacement of the peak at the maximum absorption.

The electrochemical activity of the $[\text{Fe}(\text{CN})_5\text{NH}_3]^{3-}$ and $[\text{Fe}(\text{CN})_5\text{CO}]^{3-}$ complexes are shown in Figure 6. Pentacyanoferrates (II) exhibit well-defined electrochemical processes that are influenced by the nature of the ligand, making it possible to modulation of redox potentials according to the donor or acceptor characteristics of the ligands.

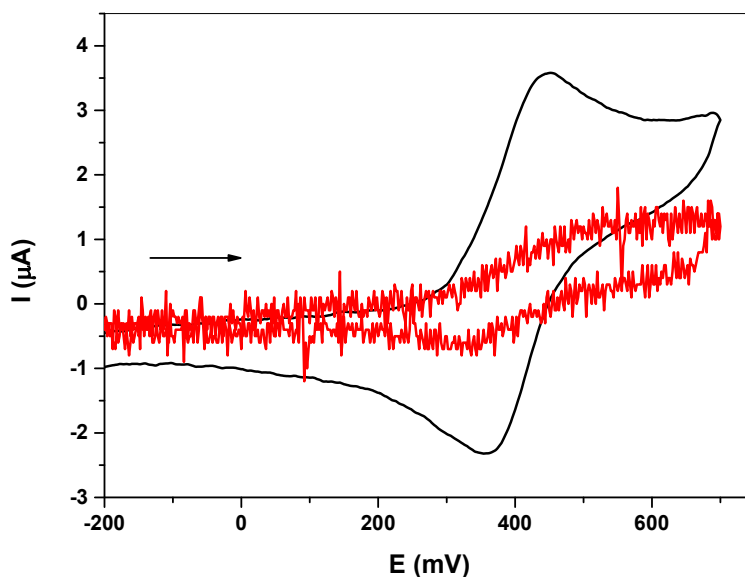


Figure 6. Voltammetry of aminopentacyanoferrate ($2.6 \times 10^{-3} \text{ mol L}^{-1}$ in KNO_3 0.2 mol L^{-1}) without the presence of carbon monoxide (in black) and in the presence of carbon monoxide (in red). Ag/AgCl/KCl saturated reference electrode, the scan of 100 mV s^{-1} , and temperature of 25°C . The arrow indicates the scan direction.

The complex presents anodic and cathodic peak potentials with values equal to 0.448 V (Fe^{2+} to Fe^{3+}) and 0.358 V (Fe^{3+} to Fe^{2+}), respectively, with current values for the anodic and cathodic peaks $3.566 \mu\text{A}$ and $-2.321 \mu\text{A}$. The potential difference between the peaks was 90 mV , with the anodic and cathodic currents ratio of 1.536 . In the literature, the $[\text{Fe}(\text{CN})_5\text{NH}_3]^{3-}$ complex in water/toluene microemulsion electrolyte, with greater ohmic resistance than the electrolyte studied in this work, showed a value of 79 mV of the potential difference between the anodic and cathodic peaks and peak current ratio of 1.11 (BALA; DASU; MIHAILCIUC, 2013; PIRES et al., 2014). The obtained voltammogram has a profile like that of Figure 6.

The $[\text{Fe}(\text{CN})_5\text{CO}]^{3-}$ complex has low electrochemical activity probably due to stabilization by the CO ligand strongly bound to Fe, which prevents the compound's redox reaction. This result also indicates that the replacement of the NH_3 ligand by the CO ligand was effective.

The factorial design 2^3 indicated that the analytical signal (Abs) is influenced by the concentration of the complex and by the agitation (30 to 120 s) at the 95% confidence level, but variations in temperature (between 15°C and 35°C) do not change the signal (Figure 7). These data show that in the complex the exchange of ligands is labile, and the thermodynamic effect is not relevant.

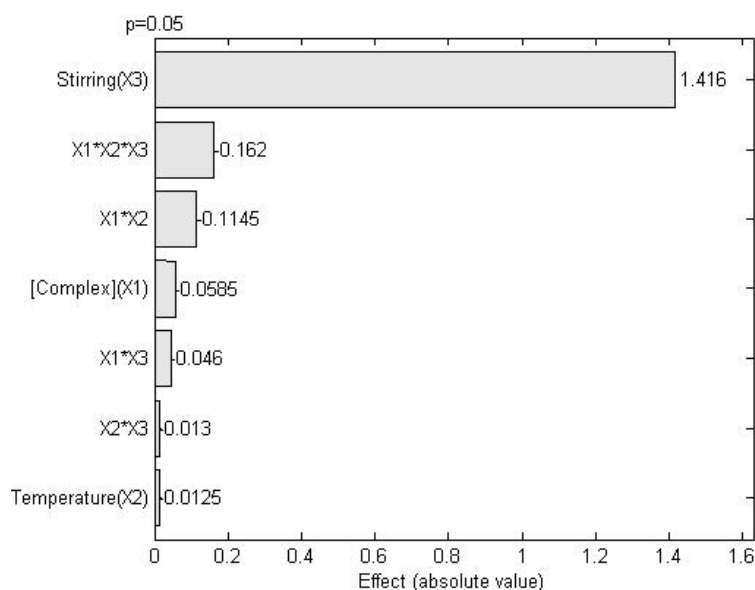


Figure 7. Pareto plot for the response in absorbance of the complex with carbon monoxide. X1) concentration of the complex; X2) Temperature; X3) stirring time. X1*X2, X1*X3, X2*X3, and X1*X2*X3 are combinations of the factors.

The aminopentacyanoferrate in solution is stable, with a decrease in absorbance at 400 nm, and 22 °C in 20 h of monitoring, of 1.95% and 1.80%, in aqueous medium and NaOH 0.1 mol L⁻¹ medium, respectively.

The absorbance of the complex is inversely proportional to the increase in the concentration of carbon monoxide (Figure 8), linear (log₁₀ function) in the range between 135 and 812 mg L⁻¹ with $R^2 = 0.9965$, showing repeatability for nine replicates in a sequence of 4.6% with the stability of the carbonylated complex of $\pm 1.0\%$ for 15 minutes after the reaction. The sensitivity of the method is 0.5337 Abs per mg of CO. The repeatability tests at three concentration levels (135, 527, and 812 mg L⁻¹ of CO) indicated an RSD between 3.1% and 4.6%. The limit of quantification is the lowest value of the analytical curve (135 mg L⁻¹) and the detection limit was determined to be 95 mg L⁻¹, employing the residual standard deviation of the analytical curve.

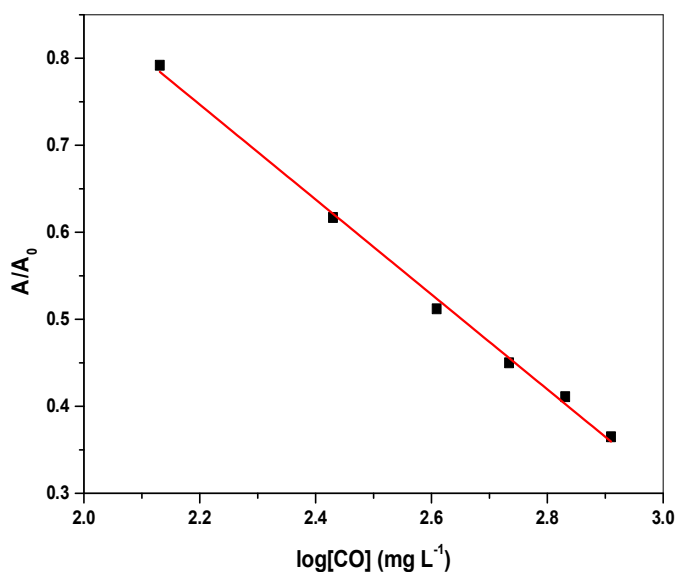


Figure 8. Analytical curve of the CO concentration with the aminpentacyanoferrate aqueous medium ($2.6 \times 10^{-3} \text{ mol L}^{-1}$), normalized by the initial absorbance value. $T = 25^\circ \text{C}$.

Figure 9 and Table 4 present the results of the selectivity of the aminpentacyanoferrate solution with different gases, except for CO_2 .

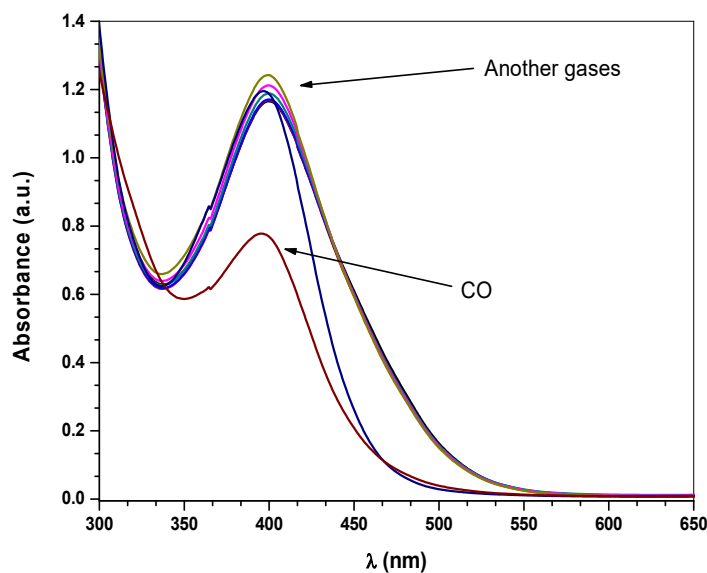


Figure 9. Molecular absorption spectrum of the aqueous solution of the aminpentacyanoferrate, at a concentration of $2.6 \times 10^{-3} \text{ mol L}^{-1}$, after bubbling the gases for 20 minutes.

Table 4 -Absorbances at $\lambda = 400$ nm, normalized to the initial value obtained from the $2.6 \times 10^{-3} \text{ mol L}^{-1}$ complex solution (blank) with the different gases studied. $\Delta\%$ = relative deviation from the initial absorbance (with N_2).

	A/ $A_0\Delta\%$
N_2	
Synt	
hetic air*	.000
H_2	0.5
CH_4	.005
NH_3	1.0
CO	.010
	5.6
	.056
	1.0
	.010
	35.0
	.650

* $20.0 \pm 0.5\% \text{ O}_2/80.0 \pm 0.5\% \text{ N}_2$

The analyte (CO) causes a decrease in absorbance and the NH_3 and H_2 do not significantly interfere in the response of the analytical signal of absorbance while CH_4 causes a 5.6% increase in the analytical signal, and a hypothesis can be due to the change in the dielectric constant of the medium, favoring the balance of Equation 4 for the species $[\text{Fe}(\text{CN})_5\text{NH}_3]^{2-}$.

The insertion of standard carbon dioxide caused a bathochromic shift to $\lambda = 445$ nm, which interferes with the analytical signal (Figure 10). This displacement may be due to the small blue formation of Prussia ($\text{Fe}_4[\text{Fe}(\text{CN})_6]_3$), catalyzed by light, in the presence of oxygen and H_3O^+ in the medium (ZHUA et al., 2020). The increase in acidity is due to the dissociation of CO_2 in aqueous media (Table 5).

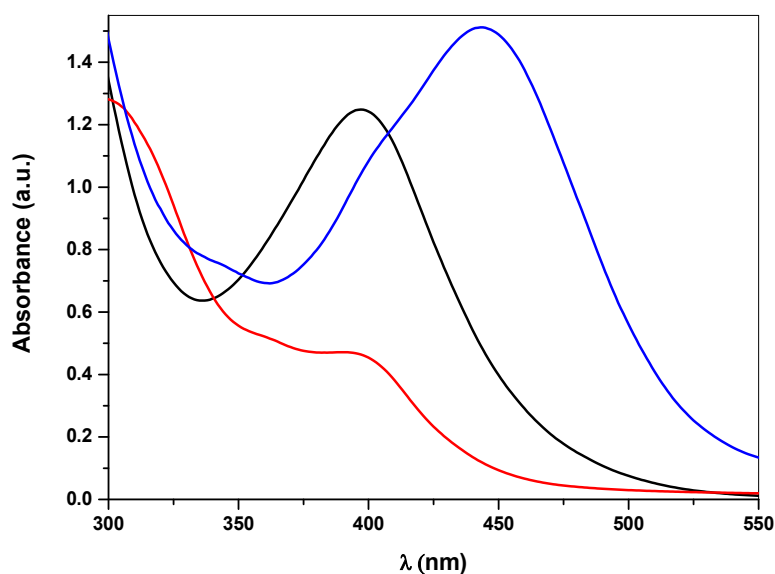


Figure 10. Molecular absorption spectrum of the aqueous solution of the aminopentacyanoferrate at a concentration of $2.6 \times 10^{-3} \text{ mol L}^{-1}$. (—) complex; (—) complex with CO; (—) complex with CO₂.

Table 5. pH of the aqueous solution of the aminopentacyanoferrate at $2.6 \times 10^{-3} \text{ mol L}^{-1}$ after bubbling for 20 minutes of N₂, synthetic air, CO, and CO₂.

Gas	Synthetic air	N ₂	CO	CO ₂
pH	9.19	9.22	9.95	6.50

In an aqueous medium saturated with synthetic air or N₂, the balance of the complex (Equation 4) with the solvent with a partial exchange of NH₃ and H₂O prevails, making it basic. In a medium saturated with CO, there is an exchange with the NH₃ ligand, releasing it in greater quantity to the aqueous medium, with an increase in pH. The difference in pH comparing the solution without CO and saturated with CO is +7.9%. In a medium saturated with CO₂, the change in pH is more pronounced, acidifying the solution due to the reaction of CO₂ in an aqueous medium generating hydronium ion (H₃O⁺).

Figure 11 shows the spectrum in the mid-infrared region for the vehicle emission gas, in which the main presence of CO and CO₂ gases are observed.

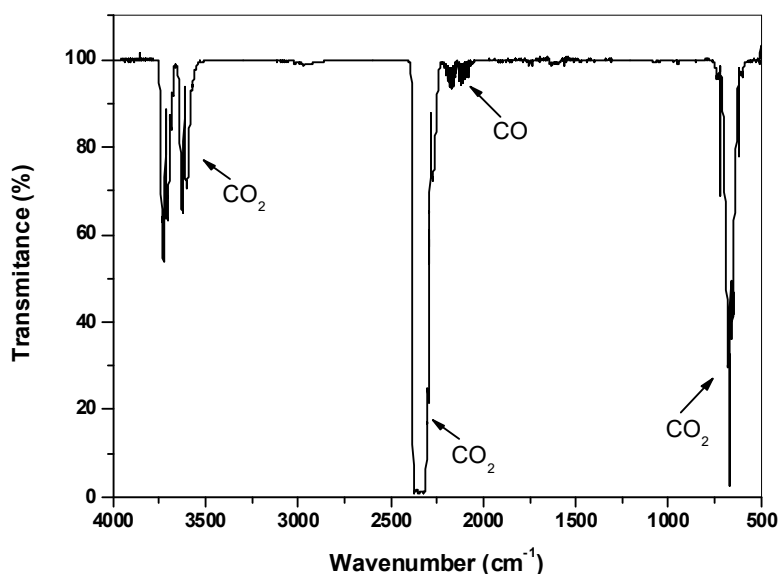


Figure 11. Spectrum in the mid-infrared of the vehicle emission gas.

The bands at 2172 and 2113 cm^{-1} refer to the vibrations of CO and the bands at 3730-3625 cm^{-1} are attributed to symmetrical stretching, the band at 2349 cm^{-1} is attributed to asymmetric stretching and the band at 669 cm^{-1} is attributed to angular deformation, all of CO_2 (KENNEY; FLYNN; GALLINI, 1961; BARAN; MULLER, 1969). The spectra in the UV-visible region show the influence of the vehicle emission gas on the absorbance of the complex (Figure 12). The pH of the solution after bubbling this gas was 6.86, because of CO_2 .

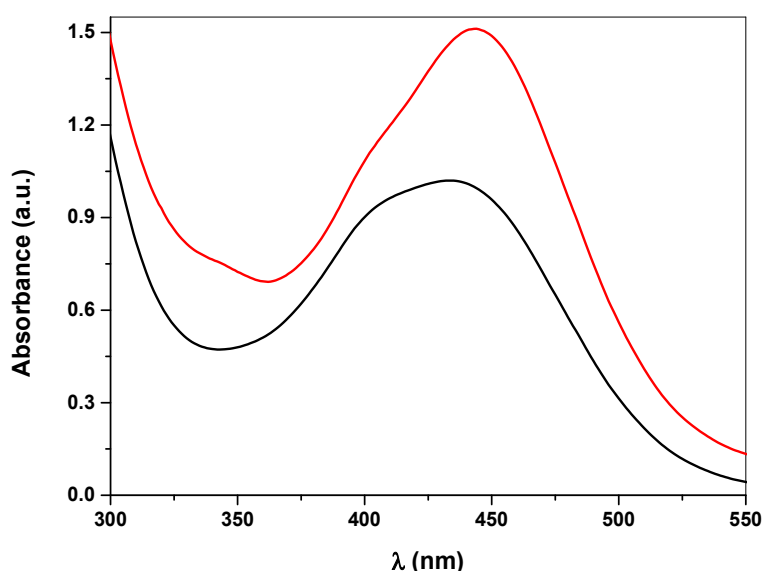


Figure 12. Absorption spectrum in the UV-visible region of the $2.6 \times 10^{-3} \text{ mol L}^{-1}$ aqueous complex with (—) CO_2 and with (—) vehicle emission gas. $\lambda_{\text{max. CO}_2} = 443 \text{ nm}$ and $\lambda_{\text{max. vehicular emission gas}} = 433 \text{ nm}$.

Changing the solvent for the vehicle emission gas measurements to 0.1 mol L⁻¹ NaOH, the maximum absorption wavelength deviation did not occur, eliminating CO₂ interference.

The proposed methodology was applied in the determination of CO in vehicle emission gases and for three gas samples, the results showed concentrations of CO of 448.10 ± 35.40 ppmv, with a relative standard deviation of 7.9 %, values below the limit of Brazilian legislation of 2,000 ppmv (BRAZIL, 2009).

4 Conclusions

The aminopentacyanoferrate can be used as a complexing agent for carbon monoxide, with absorption in the visible region, allowing a low cost analytical method, easy to apply and that can increase the control of CO emission by motor vehicles, by increasing the amounts of emission gas samples analyzed. As other gases tested do not interfere with the compound, except CO₂, aminopentacyanoferrate can be a reagent in the determination of carbon monoxide in vehicle emissions, provided that the electrolyte used is NaOH 0,1 mol L⁻¹.

Acknowledgments

This study was financed in part by the Coordenação de Aperfeiçoamento de Pessoal de Nível Superior – Brasil (CAPES); Conselho Nacional de Desenvolvimento Científico e Tecnológico (CNPq) and Fundação Araucária de Apoio ao Desenvolvimento Científico e Tecnológico do Estado do Paraná.

Conflict of Interest: The authors declare that they have no conflict of interest.

References

ABI-ESBER, L.; EL-FADEL, M.; SHIHADDEH, A. Comparison of trip average in-vehicle and exterior CO determinations by continuous and grab sampling using an electrochemical sensing method. **Atmospheric Environment**. v.41, p.6087-6094, 2007. DOI: [10.1016/j.atmosenv.2007.05.020](https://doi.org/10.1016/j.atmosenv.2007.05.020).

AMAULY, J. I.; VARETTI, E. L.; AYMUNINO, P. J. TGA-DTA and infrared spectra of potassium nitroprusside dihydrate: K₂Fe(CN)₅NO]. 2H₂O. **J. Phys. Chem. Solid**. v.46, p.1153-1161, 1985. DOI: [10.1016/0022-3697\(85\)90144-1](https://doi.org/10.1016/0022-3697(85)90144-1).

AMAULY, J. I.; VARETTI, E. L.; AYMUNINO, P. J. DTA-TGA, crystal, and molecular structure determination and vibrational studies of potassium nitroprusside sesquiquarterhydrate, K₂[Fe(CN)₅NO] 1.25 H₂O. **Journal of Crystallographic and Spectroscopic Research**. v.16, p.537-555, 1986. DOI: [10.1021/ic50088a016](https://doi.org/10.1021/ic50088a016).

BALA, D.; DASU, P.; MIHAILCIUC, C. Middle Phase Electrochemistry of Two Pentacyano(L) Ferrates(II). **Croatica Chemica Acta**. v.86, p.151-158, 2013. DOI: [10.5562/cca1999](https://doi.org/10.5562/cca1999).

BARAN, E. J.; MULLER, A. Über Na₅[Fe(CN)₅SO₃]. Eigenschaften und Untersuchung des Zerfalls in wässriger Lösung. **Zeitschrift für Anorg. und Allg. Chemie**. v.368, p.144-154, 1969. DOI: [10.1002/zaac.19693680306](https://doi.org/10.1002/zaac.19693680306).

BRAZIL. CONAMA Resolution 491/2018. Accessed in 02/02/2020. Web page <http://www2.mma.gov.br/port/conama/legiabre.cfm?codlegi=740>. (In Portuguese).

BRAZIL. Resolution 415/2009. Accessed in 02/02/2020. Web page <http://www2.mma.gov.br/port/conama/legiabre.cfm?codlegi=615>.

BRAZIL. ABNT NBR 6601/2012. Light motor vehicles - Determination of hydrocarbons, carbon monoxide, nitrogen oxides, carbon dioxide and particulate matter in the exhaust gas. 2012. (In Portuguese).

BRAZIL. CONAMA Resolution 18/1986. (In Portuguese).

BRAZIL. ABNT NBR 13539/1995. Accessed in 18/03/2020. Web page <https://www.abntcatalogo.com.br/norma.aspx?ID=4760>. (In Portuguese).

DOWNS, J. Carbon monoxide exposure: autopsy findings. PAYNE-JAMES, J.; BYARD, R. W. In: **Encyclopedia of Forensic and Legal Medicine**. 2nd edition. Oxford, UK: Elsevier, 2016, p. 444-460.

EC. European Commission. Environment. Air Quality Standards. Accessed in 01/04/2020. Web page <http://ec.europa.eu/environment/air/quality/standards.htm>.

GARCIA, L. F. A.; CORRÊA, S. M.; PENTEADO, R.; DAEMME, L. C.; GATTI, L. V.; ALVIM, D. S. "Measurements of Emissions from Motorcycles and Modeling Its Impact on Air Quality." **J. Braz. Chem. Soc.** v.24, p.375-384, 2013. DOI: [10.5935/0103-5053.20130048](https://doi.org/10.5935/0103-5053.20130048).

GUARDANI, M. L. G.; MURAMOTO, C. A. Air quality in the state of São Paulo. São Paulo: Cetesb, 2019. 228p. (In Portuguese).

KACEMA, M.; ZAGHDOUDI, K.; MORALES-RUBIO, A.; de la GUARDIA, M. Preliminary results on the influence of car characteristics on their gas emissions using gas sensors. **Microchemical Journal**, v.139, p.69-73, 2018. DOI: [10.1016/j.microc.2018.02.022](https://doi.org/10.1016/j.microc.2018.02.022).

KENNEY, D. J.; FLYNN, T. P.; GALLINI, J. B. Reaction of Ferropentacyanamines. **Journal of Inorganic and Nuclear Chemistry**. v.20, p.75-81, 1961. DOI: [10.1016/0022-1902\(61\)80462-4](https://doi.org/10.1016/0022-1902(61)80462-4).

PAPADOPOULOS, G.; NTZIACHRISTOS, J.; TZIOURTZIOUMIS, C.; KERAMYDAS, C.; LO, T-S.; NG, K-L.; WONG, H-L. A.; WONG, C. K-L. Real-world gaseous and particulate emissions from Euro IV to VI medium duty diesel trucks. **Science of the Total Environment**. v.731, p.139137, 2020. DOI: [10.1016/j.scitotenv.2020.139137](https://doi.org/10.1016/j.scitotenv.2020.139137).

PAVIA, D. L.; LAMPMAN, G. M.; KRIS, G. S.; VYVYAN, J. R. **Introdução à Espectroscopia**. Tradução da 4^a edição americana, 2010.

PIRES, B. M.; JANNUZZI, S. A. V.; FORMIGA, A. L. B.; BONACIN, J. A. Prussian Blue Films Produced by Pentacyanidoferrate(II) and Their Application as Active Electrochemical Layers. **Eur. J. Inorg. Chem.** N.34, p.5812-5819, 2014. DOI: [10.1002/ejic.201402760](https://doi.org/10.1002/ejic.201402760).

POCHWAŁA, S.; GARDECKI, A.; LEWANDOWSKI, P.; SOMOGYI, V.; ANWEILER, S. Developing of Low-Cost Air Pollution Sensor. Measurements with the Unmanned Aerial Vehicles in Poland. **Sensors**. v.20, p.3582-3599, 2020. DOI: [10.3390/s20123582](https://doi.org/10.3390/s20123582).

REBOUL, C.; BOISSIÈRE, J.; ANDRÉ, L.; MEYER, G.; BIDEAUX, P.; FOURET, G.; FEILLET-COUDRAY, C.; OBERT, P.; LACAMPAGNE, A.; THIREAU, J.; CAZORLA, O.; RICHARD, S. Carbon monoxide pollution aggravates ischemic heart failure through oxidative stress pathway. **Scientific Reports**, 7:39715. DOI: [10.1038/srep39715](https://doi.org/10.1038/srep39715).

SAFARIANZENGIR, V.; SOBHANI, B.; YAZDANI, M. H.; KIANIAN, M. Monitoring, analysis and spatial and temporal zoning of air pollution (carbon monoxide) using Sentinel-5 satellite data for health management in Iran, located in the Middle East. **Air Quality, Atmosphere & Health**.v.13, p.709-719, 2020. DOI:[10.1007/s11869-020-00827-5](https://doi.org/10.1007/s11869-020-00827-5).

SEVINC, H.; HAZA, H. Investigation of performance and exhaust emissions of a chromium oxide coated diesel engine fueled with dibutyl maleate mixtures by experimental and ANN technique. **Fuel**. v.278, p.118338, 2020. DOI: 10.1016/j.fuel.2020.118338.

SILVERSTEIN, R.; WEBSTER, F. X.; LIEMLE, D. J. **Identificação Espectrométrica de Compostos Orgânicos**. 7 ed., São Paulo: LTC,2006.

TÉLLEZ, J.; RODRÍGUEZ, A.; FAJARDO, A. Contaminacion por monóxido de carbono: un problema de salud ambiental. **Revista de Salud Publica**. v.8, p.108-117, 2016.

YANG, Q.; SHEN, H.; LIANG, Z. Analysis of particulate matter and carbon monoxide emission rates from vehicles in a Shanghai tunnel. **Sustainable Cities and Society**, v.56, 102104, 2020. DOI: 10.1016/j.scs.2020.102104.

WHO. World Health Organization, Air Pollution. Accessed in 09/01/2020. Web page https://www.who.int/gho/phe/outdoor_air_pollution/burden/en/.

ZDZISŁAW, C.; JAKUB, L.; JACEK, B.; PIOTR, W. Correlational investigation of air pollutant emissions and fuel consumption of motor vehicle in various dynamic conditions. **Global NEST Journal**. v.22, p.275-279, 2020. DOI: [10.30955/gnj.002893](https://doi.org/10.30955/gnj.002893)

ZHUA, H.; MCCAFFERYB, C.; YANGA, J.; LIB, C.; KARAVALLAKISA, G.; JOHNSONA, K. C.; DURBINA, T. D. Characterizing emission rates of regulated and unregulated pollutants from two ultra-low NOx CNG heavy-duty vehicles. **Fuel**. v.277, p.118192, 2020. DOI: [10.1016/j.fuel.2020.118192](https://doi.org/10.1016/j.fuel.2020.118192).

ZUAS, O.; BUDIMAN, H. Estimating precision and accuracy of GC-TCD method for carbon dioxide, propane and carbon monoxide determination at different rate of carrier gas. **Hemijaska Industrija**. v.70,p.451-459, 2015. DOI: [10.2298/hemind150315051z](https://doi.org/10.2298/hemind150315051z).